Effect of Zn Additives to the Electrolyte on the Corrosion and Cycle Life of Some AB_5H_x Metal Hydride Electrodes

Sanjeev Mukerjee,* James McBreen,* Gordana Adzic, John R. Johnson,* and James J. Reilly*

Brookhaven National Laboratory, Department of Applied Science, Upton, New York 11973, USA

Mariza R. Marrero and Manuel P. Soriaga**

Department of Chemistry, Texas A&M University, College Station, Texas 77843, USA

Michael S. Alexander, Arnaldo Visintin,* and Supramaniam Srinivasan**

Center for Electrochemical Systems and Hydrogen Research, Texas Engineering Experiment Station, Texas A&M University, College Station, Texas 77834, USA

ABSTRACT

Investigation on a series of AB_5-type metal hydride electrodes reveals significant improvement of cycle life in the presence of zincate electrolytes (0.5 *M* ZnO in 6 *M* KOH) for alloys without substituents such as Ce. For alloys containing Ce, which are known to impart passive protection against corrosion no additional advantage was derived by using zincate electrolytes. X-ray absorption near-edge structure investigation at the Ni K edge, due to its relative high abundance and catalytic importance in the hydriding process, was used to elicit the corrosion characteristics as a function of cycling. The spectra averaged over the bulk of the sample (transmission mode) and those from the top 200 to 250 Å (electron yield mode) indicate significant lowering of corrosion and buildup of $Ni(OH)_2$ in non-Ce substituted alloys when using zincate electrolytes. In Ce substituted samples this effect was marginal.

Introduction

The cycle of life of metal hydride electrodes is determined primarily by the corrosion and disintegration of alloy during cycling. The primary mechanism as suggested by Willems and Buschow[1] is by stress cracking during cycling resulting in rapid pulverization of the alloy particles. Hence parameters such as the molar volume of hydrogen V_H (volume expansion Å^3/H atom) and percent volume expansion during hydriding determine the cycle life characteristics. The elastic properties of the alloy also play a role as shown previously by Sakai *et al.*,[2] who have shown that softer and more ductile alloys have better cycle life characteristics. Previous reports[3-5] have also shown that substitution of the La (A component) in AB_5 alloys with small amounts of Ce result in dramatic improvements in the cycle life of the alloy. In this case it was shown that the Ce oxides (CeO_2) provide a passive film protection, although alloy decrepitation still occurs via stress cracking. Such passive film formation and corrosion inhibition has been reported previously in Al[6] and mild steel.[7]

Recent reports have shown the beneficial effects of ZnO in electrolyte[8] and as additives to the alloy,[9] in terms of improvements in cycle life. These previous reports have speculated on the ability of Zn to reduce surface corrosion of the alloying components. The ability of Zn, used as an additive, in electrolytes to reduce corrosion of steel has been shown before.[10] Drazic and Vorkapic have shown that Zn ions in the electrolyte inhibit the hydrogen evolution reaction on iron.[11] They speculated that the effect may be due to underpotential deposition of Zn on the metal. This was later shown to be the case for iron in KOH electrolyte with and without zincate.[12]

In this investigation we studied the effect of Zn ions in the electrolyte on the cycle life of some AB_5-type metal hydride electrodes. The near-edge part of the x-ray absorption spectra, x-ray absorption near-edge structure (XANES) was used to elucidate the corrosion characteristics of the individual elements in the alloy as a function of electrochemical cycling with and without the presence of ZnO in the electrolyte. XANES provided the unique ability to simultaneously probe in an element specific manner, both the bulk and the near-surface corrosion. It was therefore particularly suited for providing information on the surface segregation and buildup of corrosion products. Use of this technique for such purposes has been demonstrated by us before in Ref 13.

* Electrochemical Society Active Member.
** Electrochemical Society Student Member.

Experimental

Four different alloy compositions were chosen for evaluation of the effect on cycle life in the presence ZnO in the electrolyte. The alloys were LaB_5, $La_{0.8}Ce_{0.2}B_5$, MmB_5, and Ce-free MmB_5 (Mm^*B_5), where $B_5 = Ni_{3.55}Co_{0.75}Mn_{0.4}Al_{0.3}$ and Mm = mischmetal from bastnasite ore with a general composition of Ce (59%), La (18%), Nd (16%), Pr (6%), Y, Fe, Ca (~1%). All alloys were prepared by arc melting under a He atmosphere and then annealed under He for 72 h. X-ray diffraction (XRD) analysis of the samples showed that they were all single-phase alloys with a hexagonal $CaCu_5$-type structure. The molar volume of hydrogen in the alloys was determined by using XRD analysis on the hydrided and unhydrided samples using methodology discussed in Ref. 3. The electrodes for cycle life measurements were prepared after gas-phase preactivation. The Brunauer, Emmett, and Teller method (BET) surface area measurements revealed a particle size in the range of 2 to 4 μm. This step produced a fine powder which eliminates thickness effects in x-ray absorption structure (XAS) data and eliminates the electrochemical activation step. Electrode composition used in these tests was in the weight ratio of 17% Teflon, 33% carbon black (Monarch 1300, Cabot Corp., USA), and 50% alloy. All electrochemical cycling experiments (Arbin battery cycler, Bryan, TX, USA) were conducted in a flooded, vented cell with 6 *M* KOH. The charge and discharge rate was C/5, the cutoff voltage on charge was 1.2 V and for discharge was 0.7 V *vs.* Hg/HgO reference. The concentration of ZnO in the 6 *M* KOH electrolyte was varied between 0.1 and 1 *M*. The XAS measurements were taken on the cycled electrodes under *ex situ* conditions using beam line X11A at the National Synchrotron Light Source (NSLS). The principle aim was to measure the extent of corrosion at the Ni K edge. Data was collected simultaneously in transmission and electron yield modes. The transmission data was averaged through the bulk of the sample and the electron yield data (total electron yield, TEY) was based on escape depths of Auger electrons which were on the average from the top 200 to 350 Å of the alloy particle surface. These escape depths were based on the more energetic KLL Auger electrons with (6.5 keV) using methodology for calculations shown in Ref. 14. The efficacy of using this methodology has been shown previously in Ref. 15. However these escape depths must be viewed with caution, since the calculations are based on single-phase thin films with uniform thickness and the samples are fine powders of varying size ranging from 2 to 4 μm. The combination of the two sets of data (surface and bulk) provided information

related to the presence of surface segregation of the element under study (Ni in this case). Methodology for XANES data analysis was based on algorithms developed at the University of Washington.[16]

Results and Discussion

As shown in Table I, the percent expansion of the various alloys plays a significant role in determining cycle life. This is based on the concept of stress cracking due to lattice expansion/contraction which results in rapid decrepitation of the particles and an initial increase in capacity (activation) followed by increased corrosion and decay in cycle life. Previous studies have shown that substitution of Ce in the A component does improve the cycle life by passivating the surface,[3-5] hence the discrepancy between the molar volume, percent volume expansion, and cycle life for $La_{0.8}Ce_{0.2}B_5$ (Table I). Cycling the samples with 0.5 *M* ZnO in the electrolyte (higher concentrations up to 1 *M* ZnO did not show any further change) shows major effects for samples without Ce substitution. There is an improvement in the cycle life for Ce free samples (LaB_5 and Ce free mischmetal) to the extent of ~45%. The Ce containing samples remained unaffected.

XANES at the Ni K edge was used to investigate the effect of Zn additives in the electrolyte on the Ni corrosion in cycled samples. Figure 1a compares XANES spectra at the Ni K edge for uncycled virgin LaB_5 in transmission and electron yield modes. The fact that there is no difference between the two spectra indicates (*i*) there is no surface segregation or oxidation of Ni in the alloy electrode before cycling and (*ii*) there is no self-absorption problems in the XAS. In either case there would be a difference in the white lines (magnitude of the absorption edge) between the transmission spectra, an average over the surface and bulk of the particle and electron yield data which is the average of the first 200 to 350 Å of the surface. A similar comparison for the other alloy electrodes gave the same results. Comparison of the XANES at the Ni K edge for LaB_5 uncycled electrode and that cycled 100 times in 6 *M* KOH indicates corrosion, as evident from the increase in the white line for the cycled sample in terms of both the transmission and electron yield spectra (Fig. 1b). The increased white line for the electron yield spectra compared to the corresponding transmission data for the cycled LaB_5 shows that there is a buildup of $Ni(OH)_2$ on the surface. Comparing this with the spectra for pure β-$Ni(OH)_2$ Fig. 1b shows that the corrosion and buildup of the Ni on the surface is in the form of $Ni(OH)_2$. This can be described on the basis of a simplified equation shown below

$$LaNi_{5-x}M_x + 2z\ OH^- \rightarrow z Ni(OH)_2 + LaNi_{5-x-z}M_x + 2ze^-$$

This buildup of $Ni(OH)_2$ on the surface of the alloy is directly related to the corrosion associated with lattice expansion and contraction during cycling. Figure 2a compares the Ni K edge transmission XANES data for the LaB_5 alloy electrode after 100 cycles in 6 *M* KOH with and without 0.5 *M* ZnO. The lower white line for the data on LaB_5 cycled with ZnO indicates that zincate ions in the electrolyte are able to lower the corrosion of Ni on the alloy electrode surface. This result correlates well with the improvement in cycle life for LaB_5 with ZnO in the electrolyte. Comparison of the electron yield data for LaB_5 electrodes after 100 cycles with and without 0.5 *M* ZnO in the electrolyte indicates that there is a significant lowering in the buildup of surface $Ni(OH)_2$ when the electrode is cycled with ZnO in the electrolyte (Fig. 2b). Hence in the case of LaB_5, the presence of zincate ions in the electrolyte results in reduced Ni corrosion and a lower buildup of the surface $Ni(OH)_2$. A similar comparison of the XANES spectra at the Ni K edge for Ce-free mischmetal Mm^*B_5 showed essentially the same trends involving the lower surface segregation and buildup of $Ni(OH)_2$ after 100 cycles with ZnO in the electrolyte.

Table I. Results of x-ray diffraction and electrochemical characterization of some AB_5 alloys with and without ZnO in the 6 *M* KOH electrolyte.

Composition	V_H Å³/H atom	%ΔV/V	Capacity loss without ZnO (mAh/gm cycle)	Capacity loss with ZnO (mAh/gm cycle)
LaB_5	3.06	17.70	0.460	0.250
$La_{0.8}Ce_{0.2}B_5$	3.21	18.10	0.130	0.120
MmB_5	3.13	14.30	0.004	0.005
Mm^*B_5	3.05	16.03	0.130	0.070

* Cerium-free mischmetal.

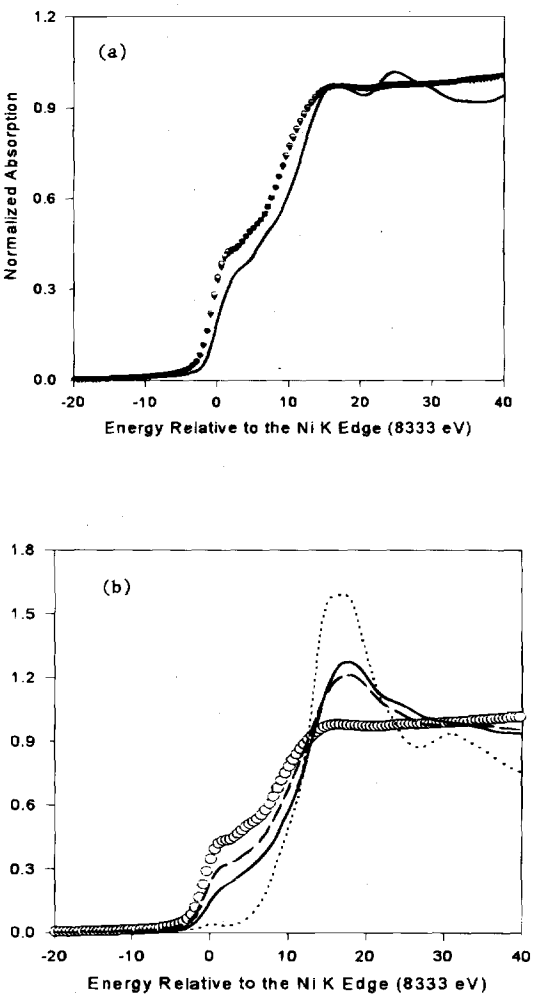

Fig. 1. XANES at the Ni K edge for (a) LaB_5 virgin sample, (○) transmission, (▼) electron yield mode relative to a Ni foil reference standard (—) and (b) LaB_5 cycled 100 times in 6 *M* KOH, (—) electron yield, (---) transmission relative to an uncycled virgin electrode (○) and β-$Ni(OH)_2$ reference standard (....).

Figure 3 shows the effect of cycling for Ce containing alloys with and without ZnO in the electrolyte taking $La_{0.8}Ce_{0.2}B_5$ as a representative case. Figure 3a shows the XANES at the Ni K edge for $La_{0.8}Ce_{0.2}B_5$ cycled in 6 *M* KOH without ZnO, in the transmission and electron yield modes. Substitution of Ce causes little change in the white line for both the spectra thereby showing that there is little surface segregation and buildup of $Ni(OH)_2$ on the alloy surface on cycling. This explains the enhanced cycle life of the Ce-substituted alloy compared to LaB_5. This fact is also exemplified by comparison with the corresponding white line for the LaB_5 electrode after 100 cycles without ZnO (Fig. 3a). Hence as shown before for MmB_5 alloys,[4] Ce imparts surface protection to the alloy by forming a passivation layer that protects against surface buildup of $Ni(OH)_2$. Comparison of the electron yield data for $La_{0.8}Ce_{0.2}B_5$ after 100 cycles with and without ZnO in the electrolyte indicates little change (Fig. 3b). This shows that the presence of zincate ions in the electrolyte does little to add to surface protection imparted by Ce in the alloy compositions. A similar analysis with MmB_5 electrodes provided the same trends. These results on the Ni corrosion compare well with the electrochemical cycling results (percent decay of capacity/cycle) in Table I.

It is therefore evident that zincate ions in the alkaline 6 *M* KOH electrolyte have the ability to impart surface protection in alloys where such passive protection does not exist. The exact mechanism by which zincate ions provide this protection is the subject of

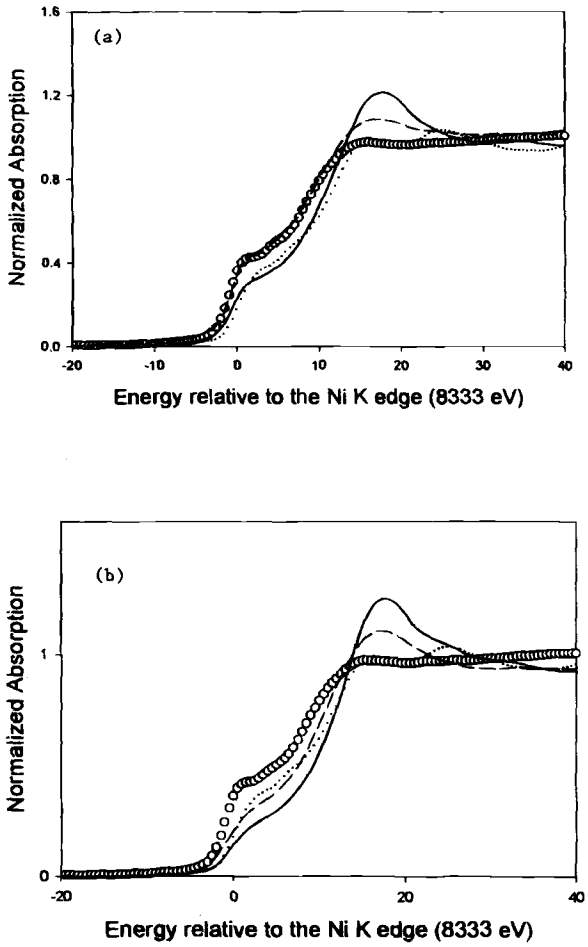

Fig. 2. XANES at the Ni K edge for LaB_5 alloy electrode cycled 100 times with (---) and without (—) 0.5 *M* ZnO in 6 *M* KOH in (a) transmission mode and (b) electron yield mode. Data for an uncycled virgin LaB_5 electrode (○) and Ni foil reference standard (...) is shown for comparison.

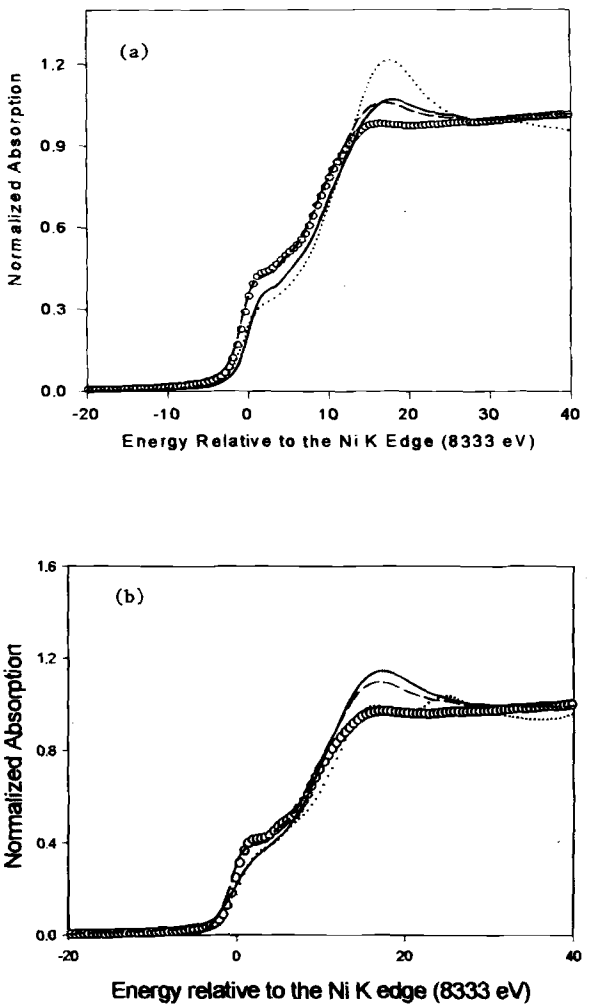

Fig. 3. XANES at the Ni K edge for (a) $La_{0.8}Ce_{0.2}B_5$ alloy electrode cycled 100 times in 6 *M* KOH, electron yield (—) and transmission mode (---), data for cycled LaB_5 (...) electrode (transmission, without ZnO) is shown for comparison and (b) electron yield data for $La_{0.8}Ce_{0.2}B_5$ cycled 100 times with (---) and without (—) 0.5 *M* ZnO in 6 *M* KOH electrolyte, data for $La_{0.8}Ce_{0.2}B_5$ uncycled electrode (○) and Ni foil reference standard (...) are shown for comparison.

our present efforts and experiments are in progress to determine the nature of the Zn species on the surface. For this purpose *in situ* XAS experiments are being conducted on the alloy electrodes at the Zn K edge. These results will be correlated with XPS data on the corresponding thin film alloy substrates. A more detailed description of these results with elucidation of the mechanism for surface protection by zincate ions will be the subject of a full paper.

Acknowledgment

The work was performed under the auspices of the U.S. Department of Energy, Division of Chemical Sciences, Office of Basic Energy Science (Contract No. DE-AC02-76CH00016, BNL and DE-FG03-93ER14381, TAMU). We acknowledge the support of the Department of Energy, Division of Material Science, Brookhaven National Laboratory (Contract No. DE-AC02-CH00016) for its role in the development and operation of the National Synchrotron Light Source (NSLS). The help of the personnel at beam line X11A is gratefully acknowledged.

Manuscript submitted May 5, 1997; revised manuscript received June 27, 1997.

Brookhaven National Laboratory assisted in meeting the publication costs of this article.

REFERENCES

1. J. J. G. Willems and K. H. J. Buschow, *J. Less-Common Met.*, **129,** 13 (1987).
2. T. Sakai, K. Ogura, H. Miyamura, K. Kurijama, A. Kato, H. Ishikawa, and C. Iwakura, *ibid.*, **161,** 193 (1990).
3. G. D. Adzic, J. R. Johnson, J. J. Reilly, J. McBreen, S. Mukerjee, M. P. S. Kumar, W. Zhang, and S. Srinivasan, *This Journal,* **142,** 3429 (1995).
4. S. Mukerjee, J. McBreen, J. J. Reilly, J. R. Johnson, G. D. Adzic, M. P. S. Kumar, W. Zhang, and S. Srinivasan, in *Proceedings of the Symposium on Hydrogen and Metal Hydride Batteries,* P. D. Bennett and T. Sakai, Editors, PV 94-27, p. 33, The Electrochemical Society Proceedings Series, Pennington, NJ (1995).
5. S. Mukerjee, J. McBreen, J. J. Reilly, J. R. Johnson, G. D. Adzic, K. Petrov, M. P. S. Kumar, W. Zhang, and S. Srinivasan, *This Journal,* **142,** 2278 (1995).
6. A. J. Davenport, H. S. Isaacs, and M. W. Kendig, *Corros. Sci.*, **32,** 653 (1991).
7. B. R. W. Hinton, Paper No. 170, Corrosion 89, New Orleans, LA, NACE (1989).
8. W. Zhang, H. F. Rogers II, and S. Srinivasan, Abstract 67, p. 87, The Electrochemical Society Meeting Abstracts, Vol. 96-1, Los Angeles, CA, May 5-10, 1996.
9. W. Zhang, S. Srinivasan, T. Shen, and R. B. Schwartz, Abstract 58, p. 77, The Electrochemical Society Meeting Abstracts, Vol. 96-2, San Antonio, TX, Oct. 6-11, 1996.
10. A. J. Appleby, H. Kita, M. Chemla, and G. Bronoel, in *Encyclopedia of the Electrochemistry of Elements,* Vol. IX A, A. J. Bard, Editor, Marcel Dekker, New York (1982).
11. D. M. Drazic and Z. Vorkapic, *Corros. Sci.,* **18,** 907 (1978).
12. J. McBreen, in *Proceedings of the Symposium on Hydrogen Storage Materials, Batteries, and Electrochemistry,* D. A. Corrigan and S. Srinivasan, Editors, PV 92-5, p. 248, The Electrochemical Society Proceedings Series, Pennington, NJ (1992).

13. S. Mukerjee, J. McBreen, G. D. Adzic, J. R. Johnson, J. J. Reilly, W. Zhang, M. P. S. Kumar, and S. Srinivasan, Abstract 642, p. 966, The Electrochemical Society Meeting Abstracts, Vol. 95-1, Reno, NV, May 21-26, 1995.
14. W. T. Elam, J. P. Kirkland, R. A. Neiser, and P. D. Wolf, *Phys. Rev. B*, **38**, 26 (1988).
15. A. N. Mansour, C. A. Melendres, S. J. Poon, Y. He, and G. J. Shiflet, *This Journal*, **143**, 614 (1996).
16. D. E. Sayers and B. A. Bunker, in *X-Ray Absorption: Principles, Application Techniques of EXAFS, SEXAFS, and XANES*, D. C. Koningsberger and R. Prins, Editors, p. 211, John Wiley & Sons, New York (1988).

Atomic Force Microscopic Imaging and Velocity Measurement of Monoatomic Terrace Motion on the (111) Cu Surface during Electrodeposition

Q. Wu* and D. Barkey**

Department of Chemical Engineering, University of New Hampshire, Durham, New Hampshire 03824, USA

ABSTRACT

Stable monoatomic terraces on the (111) Cu surface were imaged by atomic force microscopy during electrodeposition. The terraces originate at screw dislocations and conform to a faceted geometry which reflects the symmetry of the (111) Cu surface. The step velocity was computed from the shift in apparent terrace widths produced as the tip passes the growth center.

Introduction

Monoatomic spiral terraces, with singular surfaces roughly 100 atoms in width, were formed by electrodeposition on the 111 surface of a copper single crystal and imaged during growth by atomic force microscopy (AFM). It has long been known that source-limited growth may proceed by the advance of spiral terraces centered on screw dislocations,[1,2] and pyramid growth associated with dislocations has been observed on the (111) Cu surface by both optical microscopy[3,4] and scanning tunneling microscopy (STM).[5] However, the images presented here show several new features which are linked to the dynamics of step motion. The shape of the terraces reflects the geometry of the lattice, and the spacing of the steps is uniform and stable. This stability is sufficiently strong that interleaved spirals are formed without bunching of the steps. In addition, the step velocity was determined with a single AFM image by measurement of the Doppler shift in apparent terrace widths, which is produced as the scanning tip passes the growth center. The velocity of step motion is shown to be a strong function of direction, a fact which contributes to the stability of the terrace shape.

Experimental

The AFM images were obtained with a Digital Instruments Nanoscope E atomic force microscope during electrodeposition from 0.01 *M* $CuSO_4$/1.0 *M* H_2SO_4/2 m*M* HCl solution. The substrate was a copper single crystal (Monocrystals) prepared by mechanical polishing with alumina paste followed by electropolishing in orthophosphoric acid and rinsing in sulfuric acid. The counterelectrode and $Hg/HgSO_4$ reference electrode were placed in separate compartments external to the AFM fluid cell, and a constant potential was applied with an EG&G PARC Model 362 potentiostat. The images were collected in height and deflection modes simultaneously.

Results and Discussion

Figure 1a is a deflection-mode image of a spiral terrace centered on a screw dislocation. The center of the spiral is the highest position in the image, and a line drawn outward from the center steps down one atomic layer each time it crosses the arm of the spiral. The spiral itself is composed of straight segments oriented with hexagonal symmetry about the growth center and connected to one another at sharp corners. Growth proceeds by outward movement of the segments as atoms are added at the step. As one expects from geometrical reasoning, the terrace is bounded by the slowest growing directions, and these are normal to the straight segments. The corners of the spiral, for example, are advancing at a higher velocity and are located at a greater distance from the center.

The strong dependence of velocity on direction stabilizes the shape of the spiral. When growth is interrupted by the presence of an irregularity in the surface, leaving a gap in the terrace, the opening is quickly filled up. The filling-in proceeds by rapid growth parallel to the undisturbed step edge which causes the terrace to close around the gap. Afterward, the terrace is again bounded by the directions of slowest growth. This can be seen in the upper right corner of Fig. 1a where a deep stationary gap has been passed by several steps. The fast-growing directions have healed the resulting opening in each step, leaving a notch bounded by the slow-growing directions. The reverse process has been reported by Suggs and Bard for dissolution on the (111) Cu surface, in which they observed steps faceted along the (211) directions.[6] In their images, a retreating step is pinned at a single point or apex and leaves a peninsula behind as it passes. The peninsula is then cut off, and turned into an island, by rapid dissolution of its connection to the terrace. They attribute the pinning to the presence of an impurity atom.

In addition to the geometric stability of the spiral shape, the step heights and spacing are stable as well. The height-mode image in Fig. 1b shows that the steps are monoatomic with heights of about 2.5 Å. The monoatomic steps persist even when two spirals grow over one another. Figure 2 shows two spirals with origins of a few nanometers apart. The terraces are interleaved and maintain a constant step spacing which persists over at least 20 steps.

The terraces in both Fig. 1 and 2 are singular in the sense that we find no evidence of island formation on them. We have observed these stable monoatomic terraces only in the presence of chloride which apparently plays a role in stabilizing terraces and oriented steps on copper surfaces by formation of ordered overlayers.[6,7]

There is some distortion of the terrace shape in Fig. 1 because the image was acquired at a finite rate while the terraces were moving. This distortion can be used to obtain the growth velocity by a simple calculation. The slow-scan direction in Fig. 1a is from bottom to top. As a result, the terraces in the lower half of the image, where the growth direction is opposite the scan direction, appear narrower than those in the upper half, where the growth and scan directions are parallel. The real step velocity v and terrace width d are related to the scan velocity v_s, the larger and smaller apparent terrace widths d'' and d' and the angle θ between the growth and scan directions by

$$v = \frac{v_s}{\cos\theta}\left[\frac{d'' - d'}{d'' + d'}\right] \quad [1]$$

and

$$d = \frac{2d''d'}{d'' + d'} \quad [2]$$

For the terraces in Fig. 1, Eq. 1 and 2 give a velocity of 1.1 nm/s and a ledge spacing of 29 nm, which correspond to a current density of about 25 $\mu A/cm^2$. The average current density in the cell was much greater, about 450 $\mu A/cm^2$. However, the current distribution

* Electrochemical Society Student Member.
** Electrochemical Society Active Member.